Академия наук
СССР

ИНСТИТУТ
КОСМИЧЕСКИХ
ИССЛЕДОВАНИЙ

Academy of Sciences
USSR

SPACE
RESEARCH
INSTITUTE

M.A.Gruntman, V.B.Leonas

EXPERIMENTAL OPPORTUNITY OF PLANETARY MAGNETOSPHERE IMAGING IN ENERGETIC NEUTRAL ATOMS

117810 Москва, ГСП-7, Профсоюзная ,84/32

Телетайп: 111325 ПАРСЕК

Москва

ACADEMY OF SCIENCES OF THE USSR
SPACE RESEARCH INSTITUTE

Recommended
for publication
by academician
G.I.Petrov

Пр-1181

M.A.Gruntman, V.B.Leonas

EXPERIMENTAL OPPORTUNITY OF PLANETARY MAGNETOSPHERE IMAGING IN ENERGETIC NEUTRAL ATOMS

1986

УДК: 523,2 + 523,6 + 539.I.074 + 62I.384.8

The experimental opportunity of planetary magnetosphere imaging in Energetic Neutral Atoms (ENAs) is considered. The potential science return of such experiment is emphasized and relevant instrumentation is discussed. The magnetosphere imaging could be performed on the basis of the developed time-of-flight technique with the use of thin foils and microchannel plate detectors. The application of the coded aperture technique is proposed, some relevant information on this technique and the principle of the aperture pattern design are presented.

Introduction

Energetic neutral atoms (ENAs), created by charge exchange collisional processes, may serve a valuable source of information on physical phenomena in planetary magnetospheres. Realization of this fact, supported by the interpretation of some experimental data on terrestrial [1] (and references therein) and Jovian and Saturnian [2] (and references therein) magnetosperes, as well as the development of the new technique to detect and identify neutral atoms [3 - 7] prompted the proposal of the new type of the experiment [1]. The basic idea is to obtain series of sequential magnetosphere "photographs" in ENAs (enagraphs). In such magnetosphere imaging experiment the spatial distribution of the neutral emitting regions for different atomic species and energy ranges of neutral atoms are to be determined. The most obvious candidates for such an experiment are the Earth and the giant planets. The instrument on board of the spacecraft orbiting at some distance from the magnetosphere, provides the detection of ENA, determines the velocity vector and identifies its type (mass) and energy (fig.1). During exposure time (say, 15 minutes) the two-dimensional picture (pictures for different masses and energy ranges) is accumulated in the memory. A

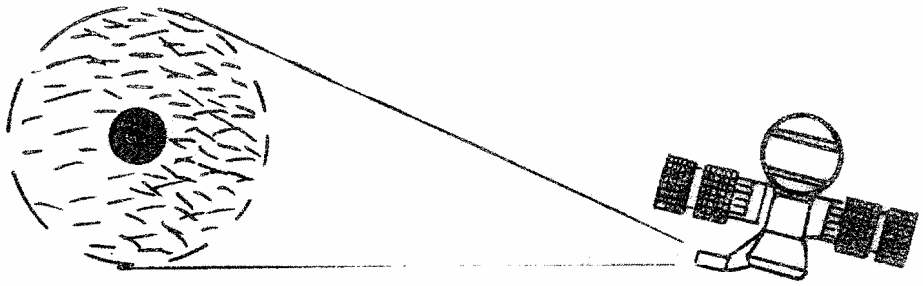

Fig.1. The instrument on-board of the spacecraft performing magnetosphere imaging in ENAs.

serie of the enagraphs (the "movies") would present the time evolution of the magnetospheric processes, for instance of the ring current decay.

The aim of this short note is to describe the general idea of the proposed experiment [1], the relevant technique and the instrument with some emphasis on the coded aperture technique. It could be considered as a first necessary step to the formulation of the full scale proposals.

Instrument principal scheme

The expected fluxes consist of atoms H and O (with some traces of He) for the Earth and H, O and S for the Jupiter. The energy range of interest is from several keV up to several hundreds keV. Until now, no final recomendations, how the instrument should look like, can be given. Nevertheless the main features are clear and similar to those described in [6,7,8].

The expected characteristics of atoms to be detected prohibit the application of the total energy detectors, say of surface barrier type, for the unambiguous atom identification. The key elements of the instrument would be thin ($\leq$ 100 Å)

selfsupporting foils and microchannel plate detectors with the abilities to determine the position of the detected particle and to fix precisely ($\lesssim$ 1 ns) the moment of the particle detection.

By measuring the times of flights in the instrument one determines only the velocity of the atom. The type (mass) of the atom or the energy can be derived from the fact that atoms of the same velocity but differing in masses interact slightly different with the thin foils. In principal, at least four effects of particle/foil interaction could serve for the identification of the atom:

- energy loss in the foil;
- scattering in the foil;
- charge state of the particle after the foil passage;
- electron emission from the foil.

The difference in the interaction of the atoms with the foils is more quantitative than qualitative. Therefore several effects are to be used simultaneously for the atom unambiguous identification.

The instrument may be built on the basis of the improved version of the detecting module developed for the neutral Solar Wind experiment [7]. This module, which will be called the basic one, is shown in fig.2 and consists of thin selfsupporting foil F, two electrostatic mirrors EM and two microchannel plate detectors D.

Energetic neutral atom A, penetrating the foil, suffers scattering (deflection), energy loss and produces electron emission from the both sides (input and exit) of the foil. These electrons are accelerated up to, say 1000 eV, by the

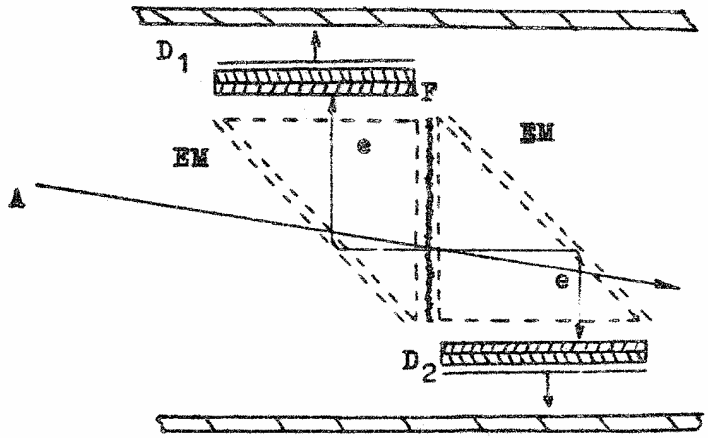

Fig.2. Basic module for the detection and identification of energetic neutral atoms. F - thin foil, EM - electrostatic mirror, D - microchannel plate detector, A - energetic neutral atom, e - secondary electron, emitted from the foil.

nearest grid, travel in the equipotential space, reflect at the outer grid and after flying a certain distance again in the equipotential space of the mirror reach finally the detector D. The assembly, which accelerates, reflects and conveys electrons from the foil to the detector, is called electrostatic mirror and is built from the high transmission (95-98 %) harp grid. Such electrostatic mirror provides isochronous transport of electrons from the foil to the detector regardless to the position of the particular point of the foil where they were emitted [7,9]. Moreover, the electrostatic mirror preserves the information on the position of the emission point and transports the whole image, formed by ENAs on the foil, to the sensitive surface of the detector D [9].

The microchannel plate detector provides precise ($\lesssim$ 1 ns) timing of the moment of the electron detection [10]. Since the electrostatic mirror assembly is isochronous device, the

moment of the foil penetration by ENA could be fixed (timed) with almost the same accuracy. The coordinates of the centre of "gravity" of the emitted from the foil electron bunch, hitting the detector D sensitive surface, could be determined providing this detector is a position-sensitive one. The most convinient for this purpose seems to be the application of the microchannel plate detector with the so-called wedge-and-strip anode [11,12]. By the accumulation of the coordinates of the sequence of the electron bunches (which correspond to the coordinates of the foil penetration points), the image, formed by ENAs at the foil surface, could be registered.

The number of electrons in the bunch could also be determined by the measurement of the pulse height at the detector output. For this purpose the detector's single electron amplitude resolution should be as narrow as possible and the electrons in the bunch should be multiplied without mutual interference. The last demand is adverse to the necessity to contain the electron bunch as compact as possible which is required for the accurate coordinates determination. The controversy could be escaped if either one microchannel plate with curved channels or the chevron stack of two straight channel microchannel plates with virtually no gap between them is used as the multiplying element in the detector D.

The described basic module would be multipurpose and would provide the possibility to determine the moment and the position of the foil penetration point by ENA as well as the number of the emitted electrons. Combining and cascading such basic modules and/or their elements, the instruments of different complexity could be designed.

The main idea of the probable scheme of the instrument for ENA imaging is depicted in fig.3. The scheme reflects an attempt to utilise the majority of the potential opportunities for the ENA identification and imaging. The instrument looks rather complex and, perhaps, too redundant and may be simplified to some extent. Further experimental study of the atom/foil interaction is needed to determine which simplifications could be made. The scheme of the instrument in its most powerful version, as shown in fig.3, is very helpful to describe the idea of the proposed technique.

The light baffle (about half meter long) defines the field of view of the instrument which may be approximately 15°. This implies that for the imaging of the area around the Earth with the diameter of 10^5 km (15 R_E, R_E - the Earth radius) the spacecraft is to be situated at the distance (3-4) 10^5 km, and the spatial resolution of the neutral emitting region (1 R_E × 1 R_E) requires the angular resolution better than ($1^{\circ} \times 1^{\circ}$).

The deflection system (DS), either of electrostatic or permanent magnet type, sweeps plasma electrons and ions out from the detecting assembly entrance window (2-3 cm in diameter).

The neutral atom passes through the nuclear track filter (NTF) [5,7] or protective film (PF) [6], two thin foils F_1 and F_2 and finally is detected by D_5. The nuclear track filter or protective film would serve to improve the atom flux (signal) to background UV photon flux (noise) ratio in the detecting assembly. Another way to protect the detecting assembly from the superior UV photon flux is to install the

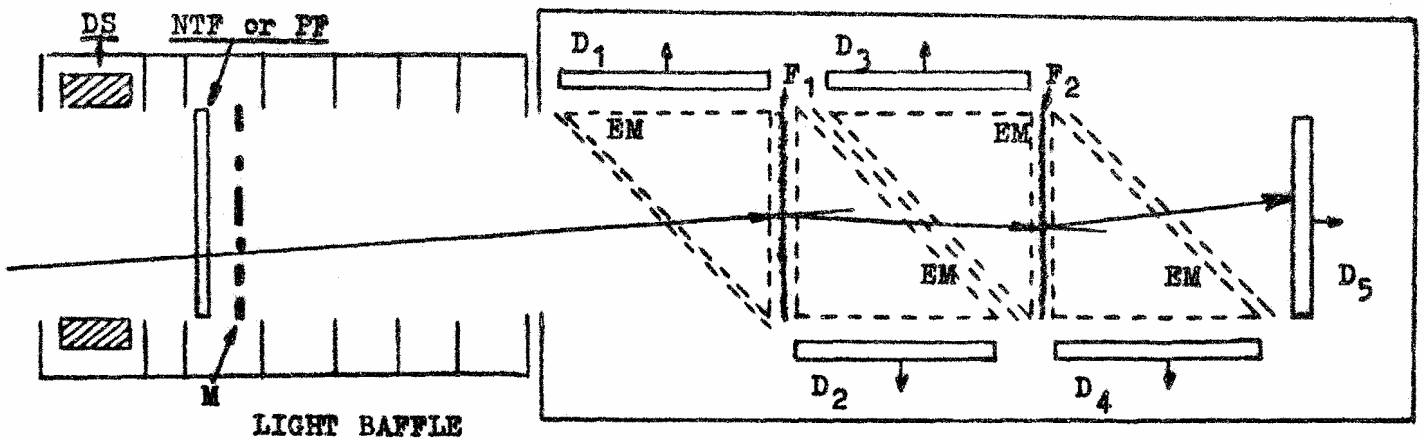

Fig.3. Instrument for magnetosphere imaging in energetic neutral atoms. DS - deflecting system (electrostatic or permanent magnet), NTF - nuclear track filter, PF - protective film, M - coded aperture mask, EM -electrostatic mirror, F_1, F_2 - thin foils, D - microchannel plate detectors

shield in the baffle covering the solid angle, where the actively emitting geocorona (for the case of the Earth) is contained. The use of the protective film puts the lower limit on the energy range of the instrument and perturbs both the atom energy and the trajectory. The nuclear track filter does not affect approximately 10 % of the atoms but the other 90 % of the atoms penetrating the bulk of the filter material are perturbed in a way similar to the protective film, though may be to a far greater extent, since the nuclear track filter thickness (1-2 μm [5,7]) is far greater than that of protective film (0.1 μm [6]). It should be noted that electron emission from the nuclear track filter surface may help to distinguish between atoms passed through the holes and the bulk of the material.

Four electrostatic mirrors pick up, accelerate and transport isochronously secondary electrons emitted from the foils to the detectors D_1, D_2, D_3 and D_4. The following values are measured:

- the pulse heights (A_1, ..., A_5) from each detector D;
- the positions $((x_1,y_1),(x_2,y_2))$ of the foil penetration points by atom;
- the position (x_3,y_3) of the point where atom arrived at D_5;
- two time intervals τ_1 and τ_2 corresponding to the times of flights between the foils and the second foil and the detector D_5.

If one assumes 64 × 64 pixels spatial resolution for the detectors D_i, 64 pulse amplitude levels, and 128 channels for both τ_1 and τ_2 measurement, then each registration of the event (ENA arrival) would produce as much as 100 bits.

It is obvious that for even modest count rates, say 10^2 s^{-1}, the information is to be treated and compressed before the transmission to the Earth.

The instrument utilizes essencially coincidence mode. For the event (ENA arrival) the pulses from all five detectors D_i must correlate strongly in time and, moreover, the coordinates measured for the input and exit surfaces of each foil must correspond to each other. Such multiple coincidence technique eliminates virtually any random coincidences even in the presence of superiour UV beackground [4,5,7].

The coordinates $((x_1,y_1),(x_2,y_2),(x_3,y_3))$ provide information on the initial velocity vector direction and the scattering in the foil; the pulse heights A_i - on the numbers of electrons emitted from the foils; and the time intervals τ_1 and τ_2 - on the atom initial velocity and the velocity (energy) loss in the second foil.

The neutral atom mass, energy and velocity vector may be determined from these measurements. The direction of the velocity vector may be deduced in such a way only if the scattering of atoms in the foils is small. This is true for relatively high energies of atoms (the "highness" of the energy is determined by the desired accuracy of the velocity direction determination). For the realistic conditions the energy of several dozens keV is not "high" enough. The ENAs with such energies are of the most interest for the proposed experiment.

If ENAs scatter too much in the foils, the coded aperture technique could be used. The special mask M consisting of the holes and opaque material is installed at the entrance of the

instrument (fig.3). The image, formed by the ENAs at the surface of the foil F_1 is registered by D_1 and/or D_2. The distribution of velocity vector directions could be derived from the stored image by the special postprocessing procedure. Obviously this technique, being implemented in the instrument for the study of the neutral Solar Wind [7], could improve drastically its quality by providing the opportunity to measure the neutral atom flux angular distribution.

Though the coded aperture technique was used a number of times in space and laboratory experiments (e.g. [13,14]), it still cannot be called well known or widespread and will be described in more details further.

Coded aperture. Principle of operation

To overcome the problem of the ENA trajectory deflection in the foil and to retain the instrument ability for imaging of such atoms, the use of the coded aperture is proposed. In this paragraph some information relevant to the coded aperture technique is given and the next paragraph shows how in practice the aperture pattern may be designed.

The most obvious way to obtain an image of the object in particles which cannot be controlled (by mirrors, electromagnetic fields etc.) is to use the pinhole camera. This is the case, for instance, for γ-rays and hard X-rays as well as for ENAs. The greater image spatial resolution, the smaller pinhole diameter should be, and the speed of image forming system may not suffice to produce an image of the desired quality. Such situation is rather typical for space experiments and magnetosphere imaging in ENAs is not an exception. To overcome the problem, the signal integration may be applied.

If one produces simultaneously N images with N pinholes, for superimposed composite image the $(N)^{1/2}$ improvement of the signal to noise ratio may be obtained.

Two possible approaches are to be outlined. In the first one the number of not overlapping, distinct images is formed by N pinholes and these images are then added to produce the image of the object. Though this approach was successfully realized in [15] for as many as 85 pinholes, the further increase in the pinhole number becomes troublesome.

In the second approach, the images formed by N pinholes, mix (multiplex), superimpose (not matching each other!) producing the meaningless and not recognizable at first glance picture which must be unscrambled by postprocessing in order to obtain the image of the object (fig.4). This multiplex image approach, pioneered in [16,17], is called the coded

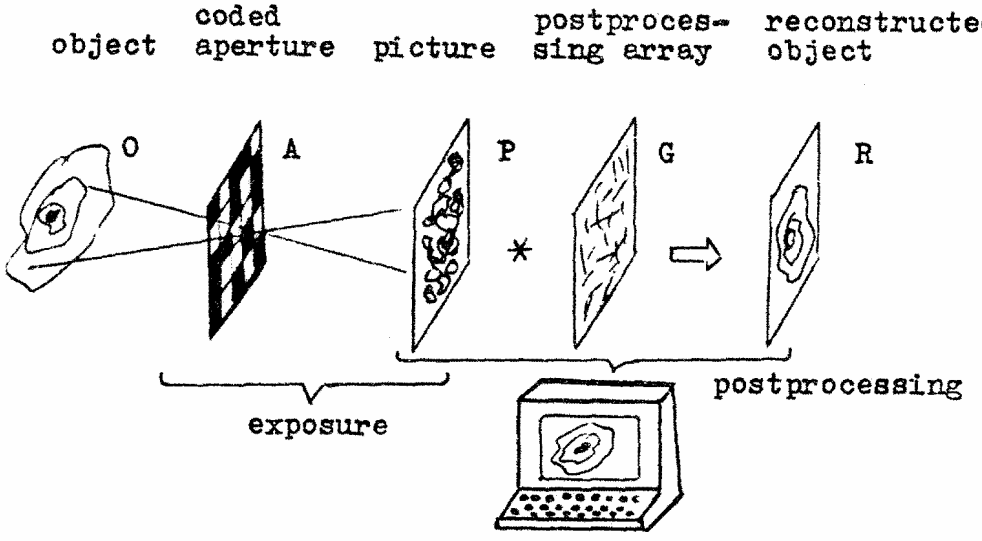

Fig.4. General scheme of the coded aperture technique.

aperture one, and may be recomended when high-resolution low photon (particle) budget photographs (enagraphs) are desired.

For the sake of complicity the application of the similar technique for one-dimensional problems is to be mentioned, where both the spatial multiplexing [18,19] and miltiplexing in time [20] are used.

Now let us consider the two-dimensional imaging technique corresponding to the scheme shown in fig.4.

The object forms the multiplexed image through the coded aperture mask on the sensitive surface of the recording device, e.g. position-sensitive detector. The digital image is then postprocessed with aid of computer to obtain the reconstructed object picture. Let the two-dimensional array O represent the object, A - aperture and P - recorded picture. Then

$$P = O*A + N \qquad (1)$$

where N - the noise and * denotes the correlation operator. The coded aperture is the certain number of elementary (assume equal) holes in certain places and A is two-dimensional binary array with elements equal to unity for hole (transmission) and to zero for the opaque material.

The use of the Fourier transform to derive O from (1) is not beneficial since small terms in Fourier transform of A would produce the noisy reconstructed image [21]. The another approach is to obtain the reconstructed image R by the convolution of P with the postprocessing binary array G (see e.g. [13,21,22])

$$R = P*G = O*(A*G) + N*G.$$

If (A*G) is a delta function, then

$$R = O + N*G$$

and the reconstructed image equals the object O in the absence of the noise (N = 0).

The quality of the imaging system usually is described in terms of the point spread function (PSF). The PSF is a reconstructed image of the object (the system "output"), for the object being delta function, and is equal to the correlation of the aperture transmission function with the postprocessing function (A*G) in our case. Even in the absence of the physical noise N, the image reconstruction with the correlation postprocessing is prone to the artifacts or inherent inaccuracy, as it was sometimes called, if PSF is not equal to the delta function. Therefore the trick is to find such aperture and postprocessing arrays, that their correlation be as close to delta function as possible.

Simple qualitative considerations may prompt the direction of the search for the desired arrays A and G. If the distant star-like object (any object may be considered as the sum of star-like radiating sources of different intensities) illuminates the aperture mask (array A), its image at the detector plane will be similar to that of the mask pattern itself. Obviously, the correlation of this image with the mask will show the central spike and sidelobes. But this correlation is the autocorrelation of the array A. The ideal case would correspond to sidelobes equal to zero. At least, they should be as flat as possible; then the image could be reconstructed by allowing for this dc level (pedestal) after postprocessing procedure. The random arrays must have the desired quality: due to their intrinsic randomness their sidelobes would be rather

flat. In such arrays 1's and 0's are situated randomly and correspond to the holes and opaque material respectively.

In the first applications different types of random arrays were used for the aperture coding design [13,16,17,19,22], but PSFs were not ideal, though the aperture arrays were subjected even to computerized iterative improvement process [13].

Afterwards few array types were found, for which PSF is delta function or delta function plus constant (dc) level (pedestal) depending on the type of particular G array. One type of the arrays is the so called nonredundant arrays (NRAs) (e.g. [23]); their autocorrelation (A*A) consists of the central spike and sidelobes perfectly equal to unity out to some lag and either unity or zero beyond that. This means, that if one considers all possible separations between holes (i.e. 1's) in A, one finds that each separation is occured only once, i.e. they are nonredundant.

The major disadvantage of NRAs is that the ratio of the number of holes to the total number of array elements (transmission or throughput) is very low. Although their nonredundancy make them ideal for the design of the systems where the number of the active elements (holes in our case) is to be minimized, as in the case, for instance, for the very large array configurations in radio astronomy [24].

Another class of arrays with good PSF and high (0.5) transmission is the so called uniformly redundant arrays (URAs) suggested first time for the two-dimensional imaging in [21]. In such arrays the number of times that particular separation occurs is constant regardless of the separation

distance. Although the arrays are redundant, but they are uniformly redundant. Autocorrelation for such an array would be the central spike plus dc level. For the illustration see the figure 7 and figure 8 (explanations further in the text) where URA and its autocorrelation are shown correspondingly.

If the URA is correlated not with itself but with the array G with elements

$$G(i,j) = 1, \text{ if } A(i,j) = 1$$
$$= -1, \text{ if } A(i,j) = 0 \qquad (2)$$

i.e. all zero elements in array A are changed to -1's to form the array G, then the PSF improves drastically. The correlation of A with G gives perfect PSF, i.e. delta function (more precisely delta function multiplied by the number of the holes or 1's in the array) with zero sidelobes. The use of G in the form (2) was suggested in [22] and such postprocessing was called general mismatch scheme. For the more general case when the aperture throughput ρ differs from 0.5, the perfect PSF could be obtained if array G with elements

$$G(i,j) = 1, \text{ if } A(i,j) = 1$$
$$= -\rho/(1-\rho), \text{ if } A(i,j) = 0$$

is used. This technique was presented the first time in [21] and called balanced correlation method.

The URAs seem to be an ideal choice for the aperture design for coded aperture imaging since they provide perfect PSF, high throughput and make feasible the reconstruction of the object without artifacts. It should be noted here, that even in the absence of physical noise (N = 0), the noise in reconstructed object R would be present due the statistical nature of the detected flux. This question, as well as the

the questions of the signal to noise ratio, optimal mask transmission ρ , tomographical opportunities were considered in detail for URA implementation and application in [25 - 27] .

The comparison of the coded aperture technique with the pinhole camera was performed in [21,22,27] . The main conclusion is that the coded aperture technique is more efficient for the imaging of the star-like objects. For extended objects (and magnetosphere represents the object of this type) their performances become equal. Nevertheless, the application of the coded aperture technique for magnetosphere imaging seems to be beneficial due to the opportunity of simultaneous imaging in both "high" and "low" energy ENAs by the same instrument. Enagraphs for "high" energy atoms could be obtained without the use of the coded aperture, since ENA initial trajectory may be accurately reconstructed. The greater is the instrument sensitive area and correspondingly the signal, the better enagraphs could be obtained. For "low" energy ENAs either coded aperture or pinhole camera should be used. For the latter case, the instrument sensitive area would be dramatically reduced resulting in very low efficiency of the instrument for "high" energy ENAs. That is why the instrument with the coded aperture seems to be very attractive for magnetosphere imaging in ENAs, both "high" and "low" energy ones.

It should be noted also that the majority of the performance assessment for the coded aperture technique were performed for the star-like objects and extensive computer simulation is still needed for the extended objects of expected magnetospheric types. The question of the reconstructed image

artifacts caused by imperfections of the coded aperture mask manufacturing, being recognized as a very serious problem [20,28,29], also requires the detailed computer simulations.

Coded aperture. Design

Let us consider briefly how the two-dimensional coded aperture pattern (URA) could be designed. The detailed description of the procedure may be found, for instance, in [30].

Let the dimensions of the array be $N_1 \times N_2$, N_1 being the number of rows and N_2 - the number of columns. It is necessary that the total number of URA elements $N_0 = N_1 \times N_2$ can be expressed as

$$N_0 = 2^{k_1 k_2} - 1$$

where URA dimensiones $N_1 = 2^{k_1} - 1$ and $N_2 = N_0/N_1$ are integer, relatively prime and greater than 1. We costruct the array with $N_1 \times N_2 = 31 \times 33 = 1023$ elements and $k_1 = 5$ and $k_2 = 2$.

The URA is constructed by the generation of the one-dimensional pseudo-random sequence of the length N_0 and mapping it in a proper way on the two-dimensional array. The technique to generate pseudo-random sequences and their characteristics are described in details in [30,31]. The pseudo-random sequence $a_0, a_1, \ldots, a_{N_0-1}$ is obtained from a primitive polynomial $h(x)$ of degree $m = k_1 \times k_2$. For $m = 10$ the primitive polynomial is $h(x) = x^{10}+x^3+1$ and the corresponding linear feedback shift register is shown in fig.5. The nonzero initial register state is necessary, the register to be started up. Assume the initial state of the each element of the shift register is 1. The sign $\oplus$ denotes addi-

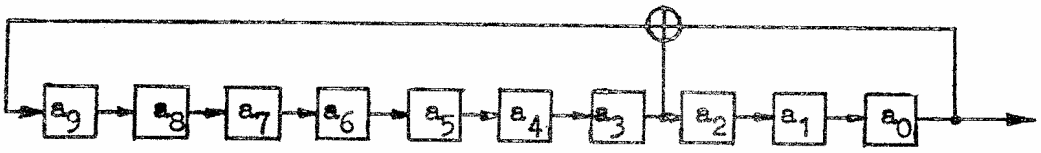

Fig.5. The linear feedback shift register corresponding to primitive polynomial $h(x) = x^{10} + x^3 + 1$. The sign ⊕ denotes addition mod 2.

tion mod 2.

After the pseudo-random sequence is generated, it should be mapped on the $N_1 \times N_2$ array. The procedure of the mapping is shown in fig.6, where first 200 (of 1023) sequence elements are positioned. The upper left corner (marked by small diamond) corresponds to the array element (1,1). The mapping is begun from this array element. The direction of the mapping is shown by the solid line. It will end in the lower right element. Each time the sequence element is mapped, the numbers of row and column are incremented by 1. While incrementing, the numbers of row and column are considered by modulo N_1 and N_2 correspondingly. This means that when the number of the row (column) reaches its ultimate value $N_1(N_2)$, the next array element, where the sequence would be mapped, will have the number of row (column) equal 1.

Figure 7 presents the resulting URA. The blackened squares correspond to 0's and white ones (holes) to 1's.

This array autocorrelation function is shown in fig.8. The height of the central spike is two times greater than the perfectly flat sidelobes - pedestal. For balanced correlation, such array provides perfect PSF with zero sidelobes, which is shown in fig.9.

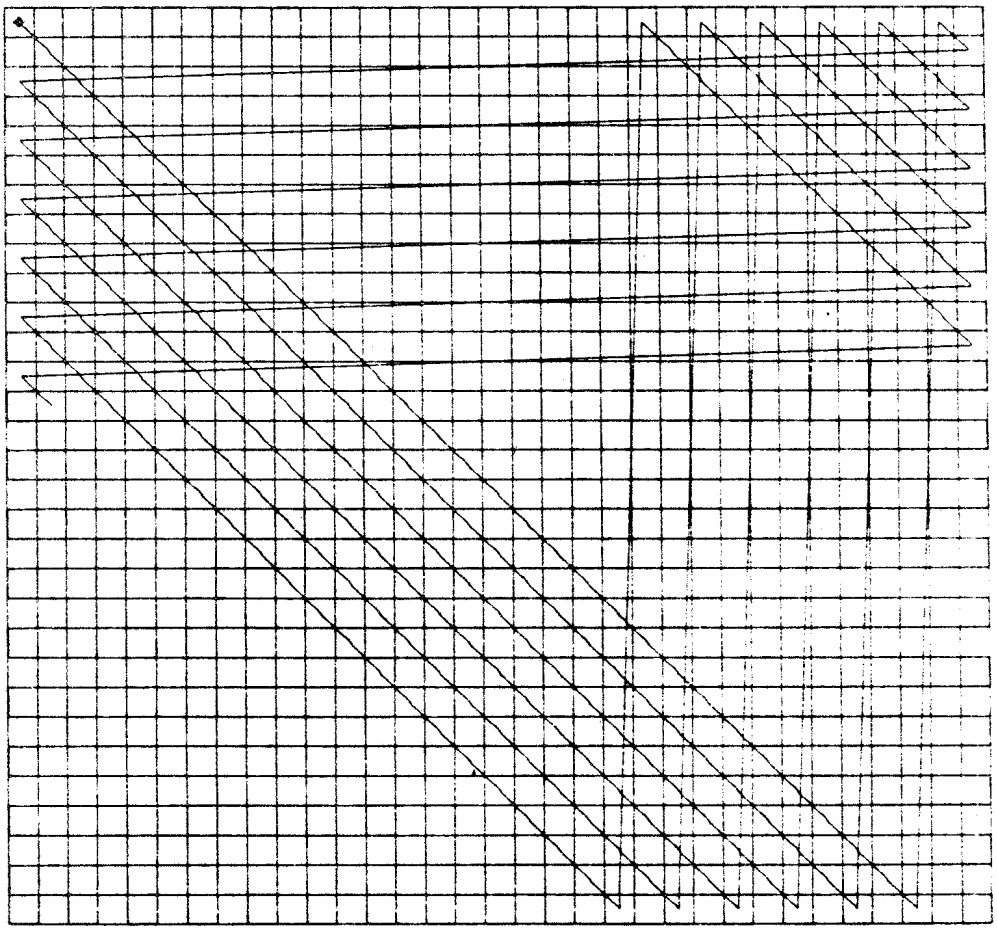

Fig.6. The sequence of the mapping one-dimensional pseudo-random elements on two-dimensional array. Upper left corner (marked by the diamond) is the starting point and corresponds to array element (1,1). Only first 200 elements are presented by the solid line. The mapping will end in the lower right corner.

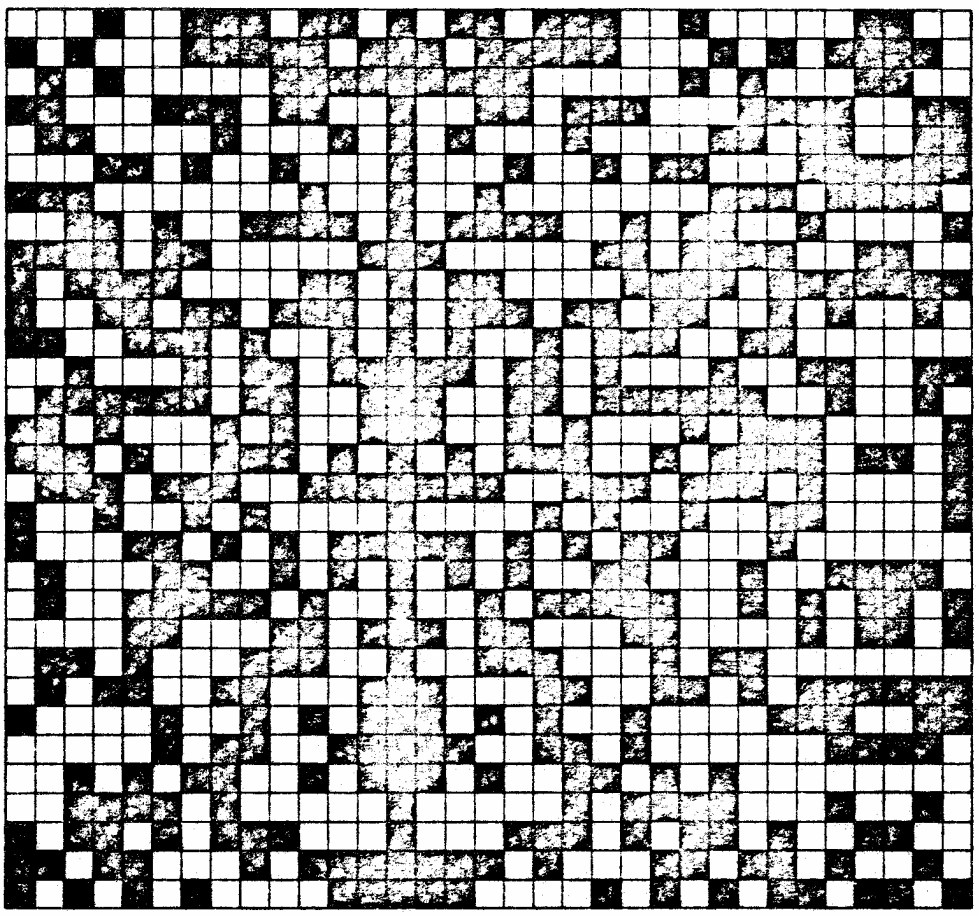

Fig.7. Constructed two-dimensional uniformly redundant array (URA). Blackened squares correspond to 0's and white ones (holes in the mask) to 1's.

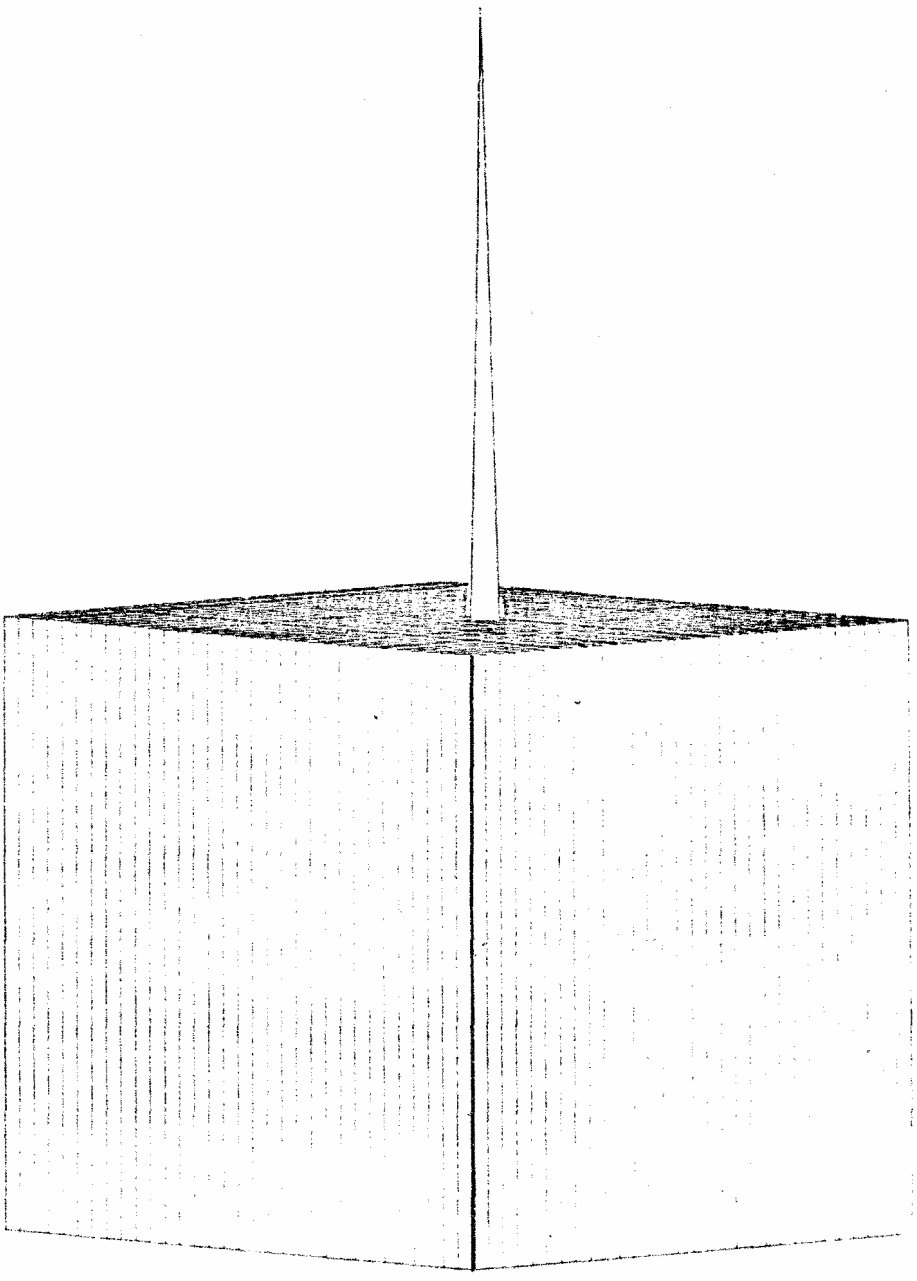

Fig.8. Uniformly redundant array autocorrelation function. Central spike is two times greater than perfectly flat sidelobes.

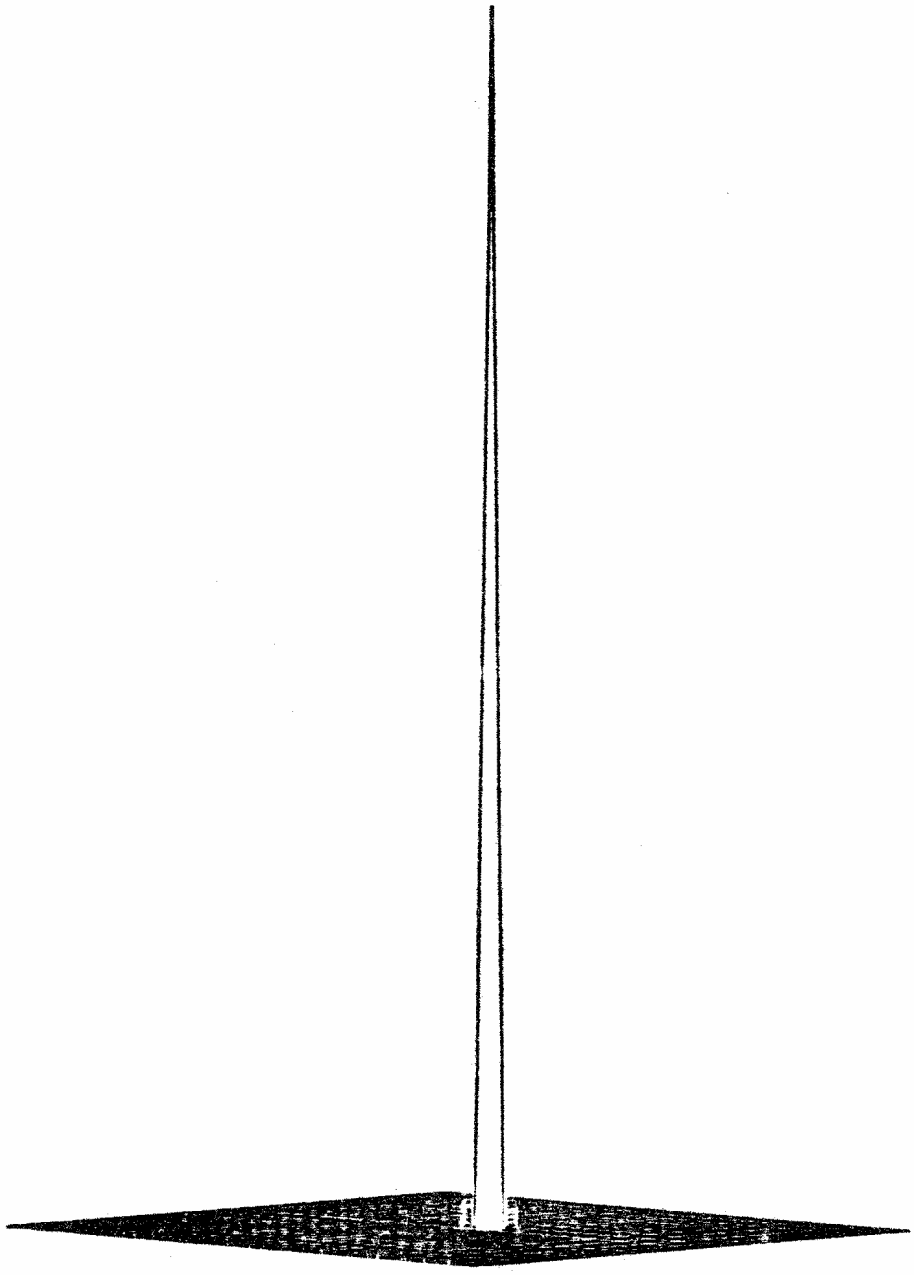

Fig.9. Ideal point spread function (zero sidelobes) of URA based imaging system with the use of balanced correlation technique.

Summary

The experimental possibilities of planetary magnetosphere imaging in ENAs are considered. The potential science return of such an experiment is emphasized and relevant instrumentation is discussed. The magnetosphere imaging could be performed on the basis of the developed time-of-flight technique with the use of thin foils and microchannel plate detectors. The application of the coded aperture technique is proposed, some relevant information on this technique and the principle of the aperture pattern design are presented.

Acknowledgement

Authors wish to express their gratitude for stimulating discussions to Academician G.I.Petrov (Space Research Institute, Moscow), Prof. S.Grzędzielski (Space Research Centre of the Polish Academy of Sciences, Warsaw), Prof. W.Axford, Dr.H.Rosenbauer and Dr. A.Richter (Max Planck Institut für Aeronomie, Lindau), Prof.D.Williams (Johns Hopkins University, Baltimore, MD) and Dr.K.Hsieh (University of Arizona, Tucson, AZ). Prof.A.Cheng (Johns Hopkins University, Baltimore, MD) is acknowledged for sending the preprints prior to publication.

REFERENCES

1. Roelof E.C., Mitchell D.G., Williams D.J. Energetic Neutral Atoms (E~50 keV) from the Ring Current: IMP 7/8 and ISEE 1. - J. Geophys. Res., 1985, v.90, No.11A, p.10991-11008.

2. Cheng A.F. Energetic Neutral Particles from Jupiter and Saturn. J. Geophys. Res., 1986, v.91, No.A4, p.4524-4530.

3. Gloeckler G., Hsieh K.C. Time-of-flight technique for particle identification at energies from 2-400 keV/nucleon.- Nucl. Instrum. and Methods, 1979, v.165, p.537-544.

4. Gruntman M.A., Morozov V.A. H atoms detection and energy analysis by use of thin foils and time-of-flight technique.- J. Phys. E: Sci. Instrum., 1982, v.15, p.1356-1358.

5. Gruntman M.A., Leonas V.B. Neutral Solar Wind. Possibility of experimental study. - Preprint 825, Space Research Institute, Academy of Sciences, Moscow, 1983.

6. McEntire R.W., Keath E.P., Fort D.E., Lui D.E., Krimdgis S.M. The Medium-Energy Particle Analyser (MEPA) on the AMPTE CCE Spacecraft. - IEEE Trans., 1985, v.GE-23, N.3, p.230-233.

7. Gruntman M.A., Leonas V.B. Possibility of Experimental Study of Energetic Neutral Atoms in Interplanetary Space.- Preprint 1109, Space Research Institute, Academy of Sciences, Moscow, 1986.

8. Hsieh K.C. Private communication, 1986.

9. Busch F., Pfeffer W., Kohlmeyer B., Schüll D., Pühlhoffer F. A position-sensitive transmission time detector. - Nucl. Instrum. and Methods, 1979, v.162, N.1-3, part 2 p.587-601.

10. Wiza J.L. Microchannel plate detectors. - Nucl. Instrum. and Methods, 1979, v.162, N.1-3, part 2, p.587-601.

11. Martin C., Jelinsky P., Lampton M., Malina R.F., Anger H. Wedge-and-strip anodes for centroid-finding position-sensitive photon and particle detectors. - Rev. Sci. Instrum., 1981, v.52, N.7, p.1067-1074.

12. Gruntman M.A. Position-sensitive detectors based on microchannel plates (Review). - Instrum. Experim. Technique (translation from Pribory i Technika Experimenta), 1984, N.1, p.1-19.

13. Blake R.L., Burek A.J., Fenimore E.E., Puetter R. Solar X-Ray Photography with Multiplex Pin-Hole Camera. - Rev. Sci. Instrum., 1974, v.45, p.513-516.

14. Fenimore E.E., Cannon T.M., Van Hulsteyn D.B., Lee P. Uniformly redundant array imaging of laser driven compression: preliminary results. - Appl. Optics, 1979, v.18, No.7, p.945-947.

15. Einighammer H.J. Detection of Weak X-Rays Sources by Image Integration. - V-th Intern. Congress on X-Ray Optics and Microanalysis, Abstracts, ed. by G. Möllenstedt and K.H.Gaukler, Springer, 1969.

16. Dicke R.H. Scatter-hole cameras for X-rays and gamma rays.- Astrophys. J., 1968, v.153, N.2, p.L101-L106.

17. Ables J.G. Fourier Transform Photography: A New Method for X-Ray Astronomy. - Proceedings of the Astronomical Society of Australia, 1968, v.1, N.4, p.172-173.

18. Nelson E.D., Fredman M.L. Hadamard Spectroscopy. - J.Opt. Soc. Am., 1970, v.60, N.12, p.1664-1669.

19. Gunson J., Polychronopulos B. Optimum design of a coded

mask X-ray telescope for rocket applications. - Mon. Not. R. Astron. Soc., 1976, v.177, p.485-497.

20. Comsa G., David R., Schumacher B.J. Magnetically suspended cross-correlation chopper in molecular beam-surface experiments. - Rev. Sci. Instrum., 1981, v.52, N.6, p.789-796.

21. Fenimore E.E., Cannon T.M., Coded aperture imaging with uniformly redundant arrays. - Appl. Optics, 1978, v.17, No.3, p.337-347.

22. Brown C. Multiplex imaging with multiple-pinhole camera.- J. Appl. Phys., 1974, v.45, No.4, p.1806-1811.

23. Golay M.J.E. Point Arrays Having Compact, Nonredundant Autocorrelations. - J. Opt. Soc. Am., 1971, v.61, N.2, p.272-273.

24. Klemperer W.K. Very large array configurations for the observation of rapidly varying sources. - Astron. Astrophys. Suppl., 1974, v.15, No.3, p.449-451.

25. Fenimore E.E. Coded aperture imaging: predicted performance of uniformly redundant arrays. - Appl. Optics, 1978, v.17, No.22, p.3562-3570.

26. Cannon T.M., Fenimore E.E. Tomographical imaging using uniformly redundant arrays. - Appl. Optics, 1979, v.18, No.7, p.1052-1057.

27. Gottesman S.R., Schneid E.J. PNP - a new class of coded aperture arrays. - IEEE Trans., 1986, v.NS-33, No.1, p.745-749.

28. Tai M.H., Harwit M., Sloane N.J.A. Errors in Hadamard spectroscopy or imaging caused by imperfect masks. - Appl. Optics, 1975, v.14, N.11, p.2678-2686.

29. Sloane N.J.A., Harwit M., Tai M.H. Systematic errors in Hadamard transform optics. - Appl. Optics, 1978, v.17, No.18, p.2991-3002.

30. MacWilliams F.J., Sloane N.J.A. Pseudo-Random Sequences and Arrays. - Proc. of IEEE, 1976, v.64, N.12, p.1715-1729.

31. Digital Communications with Space Applications. Ed. by S.W.Golomb, Prentic Hall Inc., Englewood Cliffs, N.J., 1964.

055/02/2

Ротапринт ИКИ АН СССР
Москва, 117810, Профсоюзная, 84/32

Т - 12247

Подписано к печати 19.09.86

Заказ 5834 Формат 61x86/8 Тираж 75 1,1 уч.изд.л